Magnetic field sensing with the kinetic inductance of a high-Tc superconductor

Magnetic field sensing with the kinetic inductance of a high-T_c superconductor

Cite as: AIP Advances **9**, 045217 (2019); https://doi.org/10.1063/1.5080798
Submitted: 12 November 2018 . Accepted: 05 April 2019 . Published Online: 16 April 2019

V. Vesterinen, S. Ruffieux, A. Kalaboukhov, H. Sipola, M. Kiviranta, D. Winkler, J. F. Schneiderman, and J. Hassel

Magnetic field sensing with the kinetic inductance of a high-T_c superconductor

Cite as: AIP Advances 9, 045217 (2019); doi: 10.1063/1.5080798
Submitted: 12 November 2018 • Accepted: 5 April 2019 •
Published Online: 16 April 2019

V. Vesterinen,[1,a] S. Ruffieux,[2] A. Kalaboukhov,[2] H. Sipola,[1] M. Kiviranta,[1] D. Winkler,[2] J. F. Schneiderman,[3] and J. Hassel[1]

AFFILIATIONS

[1]VTT Technical Research Centre of Finland Ltd., QTF Centre of Excellence, P.O. Box 1000, FI-02044 VTT, Finland
[2]Department of Microtechnology and Nanoscience—MC2, Chalmers University of Technology, SE-41296 Gothenburg, Sweden
[3]MedTech West and the Institute of Neuroscience and Physiology, University of Gothenburg, SE-40530 Gothenburg, Sweden

[a)]visa.vesterinen@vtt.fi

ABSTRACT

We carry out an experimental feasibility study of a magnetic field sensor based on the kinetic inductance of the high critical temperature (high-T_c) superconductor yttrium barium copper oxide. We pattern thin superconducting films into radio-frequency resonators that feature a magnetic field pick-up loop. At 77 K and for film thicknesses down to 75 nm, we observe the persistence of screening currents that modulate the loop kinetic inductance. We report on a device with a magnetic field sensitivity of 4 pT/$\sqrt{\text{Hz}}$, an instantaneous dynamic range of 11 μT, and operability in magnetic fields up to 28 μT. According to the experimental results the device concept appears attractive for sensing applications in ambient magnetic field environments.

The kinetic inductance of superconductors has found many applications in fields as diverse as bolometry,[1,2] parametric amplification,[3,4] current detectors,[5] and sensing of electromagnetic radiation,[6,7] to name but a few. Each device harnesses a certain type of a non-linearity of the kinetic inductance L_k, such as that induced by temperature, electric current, or non-equilibrium quasiparticles. In sensor applications, radio-frequency (rf) techniques are often employed in observation of the variations of L_k: a high sensitivity follows from the intrinsically low dissipation of the superconductors, manifesting itself as a high quality factor of resonator circuits, for example.

The general advantages common to all L_k sensors include a simple fabrication process involving only a single superconducting layer, and the ability to use frequency multiplexing[6,8] for the readout of large sensor arrays. These aspects have motivated the development of kinetic inductance magnetometers (KIMs), devices that combine the L_k current non-linearity with magnetic flux quantization.[9,10] In this Letter, we demonstrate KIMs fabricated from yttrium barium copper oxide (YBCO). YBCO is a high critical temperature (high-T_c) superconductor that enables KIM operability in liquid nitrogen.

Non-linear L_k of YBCO has previously been evaluated for bolometric[2] (direct[7]) detection of infrared (optical) radiation. A further benefit of the material is its high tolerance against background magnetic fields, which has recently culminated in a YBCO rf resonator with a quality factor of about 10^4 at a temperature $T < 55$ K and at a magnetic flux density of 7 T applied parallel to the superconducting film.[11] From a sensitivity viewpoint, an important benchmark for our KIM are state-of-the-art YBCO SQUID magnetometers[12] that have a sensitivity better than 50 fT/$\sqrt{\text{Hz}}$. However, these SQUIDs suffer from a complicated Josephson junction fabrication process that makes mass production difficult, and in order to extend the magnetometer dynamic range beyond a few nT, they need to be operated in a flux-locked loop requiring at least four wires to each cold sensor. KIMs typically have a higher dynamic range, and they enable operation in demanding ambient magnetic field conditions.

We review the KIM operating principle, starting from the L_k current non-linearity,[13,14]

$$L_k = L_{k0}\left[1 + \left(I_s/I^*\right)^2\right]. \quad (1)$$

In anticipation of using it for magnetometry, we have introduced a screening current I_s, the flow of which is enforced by magnetic

flux quantization. L_{k0} is the kinetic inductance at $I_s = 0$, and I^* is a normalizing current on the order of the critical current I_c. Assuming that L_k is a property of a superconducting loop with an area A, we formulate the flux quantization as

$$(L_g + L_k)I_s - B_0 A = m\Phi_0, \tag{2}$$

where L_g is loop geometric inductance, B_0 the spatial average of the magnetic flux density threading the loop, and $m\Phi_0$ an integer times the magnetic flux quantum. Sensitive magnetometry calls for a decent kinetic inductance fraction $\alpha_k = L_k/(L_g + L_k)$, and an effective method of observing the B_0-induced inductance variations. To establish an rf readout, two opposite edges of the loop are connected with a capacitor that leaves I_s unperturbed, but creates an rf eigenmode together with the loop inductance. Then, the inductance variation translates into a changing resonance frequency, a quantity which is probed by coupling the resonator weakly into a 50-Ω readout feedline. Two KIMs of this kind have recently been reported: the materials of choice have been NbN[9] and NbTiN,[10] both of which are low-T_c superconductors whose disordered nature provides a magnetic penetration depth[15] λ exceeding several hundreds of nm. For films with a thickness $d \ll \lambda$, the kinetic surface inductance equals $\mu_0\lambda^2/d$, with μ_0 the vacuum permeability.

In the design of our high-T_c KIM [Fig. 1(a) and supplementary material], we use as a guideline the theoretical responsivity on resonance[9]

$$\left|\frac{\partial V}{\partial B_0}\right| = \frac{Q_t^2 V_{in} I_s A}{4Q_e L_{tot} I^{*2}[1/\alpha_k + 3(I_s/I^*)^2]} \tag{3}$$

that describes how the magnetic field sensitivity of the resonator voltage V is related to the electrical and geometric device parameters. The readout rf power P_{rf} arriving at the KIM is expressed through an excitation voltage amplitude V_{in}. Q_t (Q_e) denotes the loaded (external) quality factor. We choose a maximal $A = (8\ \text{mm})^2$ allowed by fabrication technology. The total inductance L_{tot} equals one quarter[9] of the loop inductance plus the contribution of the parasitic trace connecting the two halves of the loop. We anticipate that reaching a significant α_k is the main bottleneck: The reported values[16] of the YBCO λ in the low-T limit are only 150 − 200 nm. Few devices have previously featured long superconducting traces with a small cross-section,[17] because this is expected to increase the probability of defects. As a compromise, we select a trace width $w = 10\ \mu$m, and compare three devices (labeled A-C) with a variable $d \leq 225$ nm. The shunt capacitor $C \simeq 16$ pF, which determines the unloaded angular resonance frequency through the relation $(L_{tot}C)^{-1/2}$, is formed from interdigitated fingers of width 10 μm and gap 5 μm. We analytically estimate that $L_g = 45.3$ nH, and the parasitic trace has a contribution of 25 − 45% of L_{tot}. The lower (upper) end of the range corresponds to a high (low) α_k. We aim at $L_{tot} \simeq 24$ nH at $\alpha_k \simeq 0.2$, and a loaded resonance frequency f_r of about 250 MHz. The f_r is chosen to be well above the magnetic signal frequencies (up to tens of kHz), while allowing the modeling of the KIM a lumped element. All device features are fabricated from YBCO.

Sample A was fabricated on a 10×10 mm^2 r-cut sapphire substrate with an yttria-stabilized zirconia and a CeO_2 buffer layer to support the epitaxial growth of a $d = 225$ nm thick YBCO film. Sapphire was initially chosen for its very low rf dielectric loss, but the deposition process of thin YBCO films is optimized for MgO.

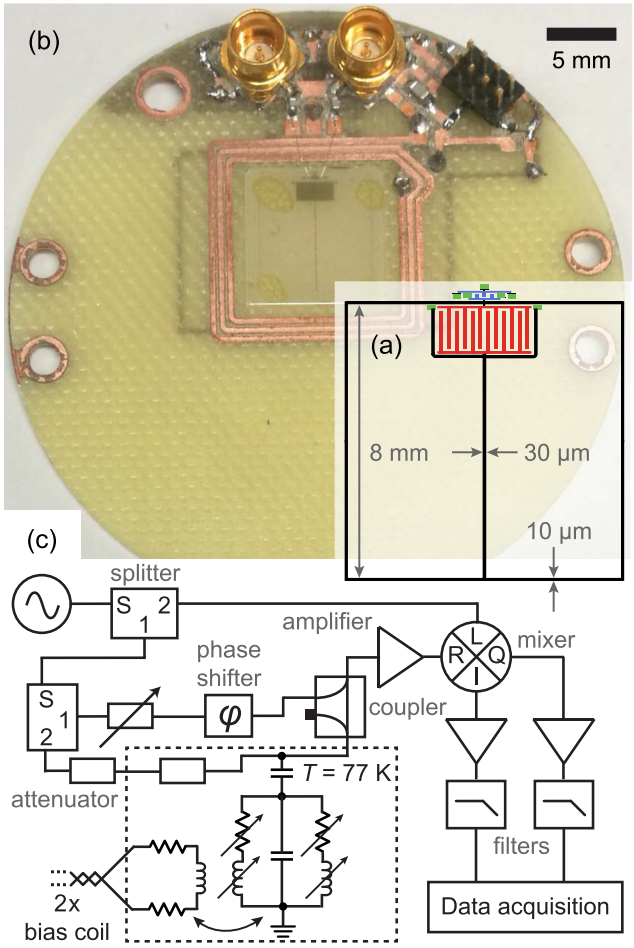

FIG. 1. Magnetometer and its readout scheme. (a) The superconductor mask layout of Sample C with a shunt capacitor, a coupling capacitor, and bondpads highlighted in red, blue and green, respectively. *The trace widths and capacitor fingers are not to scale.* (b) A photograph of Sample C on a sample holder PCB. The 44-mm-diameter PCB hosts a three-turn dc bias coil on its top surface, and a single-turn ac bias coil at the bottom. The calculated mutual inductance between the superconducting loop and the dc (ac) coil is 20 nH (5.3 nH). (c) A simplified rf readout schematic where three copies of an rf carrier are taken to ensure phase stability. The resonator encodes the magnetic signal into the rf domain. The signal appears as sidebands of the first copy of the rf carrier at low temperature T. Before amplification, the (optional) second copy interferometrically cancels carrier power. The third copy is a reference used in the demodulation of the magnetic signal to dc.

Consequently, Samples B and C with a $d = 50$ nm and 75 nm thick YBCO film, respectively, were fabricated on a 110 MgO substrate without buffer layers. Low-loss microwave-resonant YBCO structures have previously been reported on both substrate materials.[7,11] The YBCO films were deposited with pulsed laser deposition (PLD) and the devices were then patterned with optical lithography using a laser writer and argon ion beam etching. The etching process was monitored with secondary ion mass spectrometry for endpoint detection. We attach the KIMs onto a printed circuit board (PCB) that has copper patterns for rf wiring and magnetic bias coils

[Fig. 1(b) and supplementary material]. Bondwires couple the KIM to the rf readout feedline.

The first KIM characterization is the measurement of the resonance lineshape and its sensitivity to the magnetic field. As L_k makes the resonator a sensitive thermometer,[2] we resort to immersion cooling in liquid nitrogen at $T = 77$ K. We use a high-permeability magnetic shield that not only protects the sample from magnetic field noise, but also prevents trapping of flux vortices during the time when T crosses T_c. The core elements of the readout electronics are a low-noise rf preamplifier followed by a demodulation circuit (IQ mixer), and analog-to-digital converters [Fig. 1(c)] (see supplementary material for detailed setup schematics). We sweep the frequency of a weak ($P_{rf} \leq$ -66 dBm) rf tone across the resonance. We simultaneously apply a static B_0 as well as a weak, magnetic ac probe tone at a frequency of 1 kHz. This frequency is well below $f_r/(2Q_t)$, the corner frequency of the KIM detection band roll-off.[9] From the averaged in-phase (I) and quadrature (Q) components of the output we extract the complex-valued transmission parameter $S_{21} = 2V/V_{in}$. In addition, we use ensemble averaging of the modulated output voltage to extract the responsivity $\partial V/\partial B_0$ corresponding to the magnetic ac probe tone.

From the best fits[18] to S_{21} we extract f_r, Q_e, and the internal quality factor Q_i. Applying B_0 shifts f_r downwards in Samples A and C [Fig. 2(a,b)], but not in Sample B which has the thinnest film. We suspect that a non-uniform film quality, leading to a small residual resistance at $T = 77$ K in one arm of the loop, prohibits the proper flux quantization. However, also Sample B reacts to an ac magnetic excitation, and at a lower $T \approx 60$ K we observe the proper dc response as well. This makes us suspect a locally suppressed T_c in the film. We convert the frequency shifts of Samples A and C (maximally − 140 kHz and − 50 kHz, or − 0.15 and − 0.30 resonance linewidths, respectively) into an equivalent change in L_{tot}. We observe a quadratic dependence of L_{tot} on B_0 [Fig. 2(e)], which is in line with Eqs. (1–2). Unlike in low-T_c KIMs,[9,10] we do not observe resetting of the sample to $I_s = 0$ [i.e., into a finite m in Eq. (2)] upon crossing a threshold B_0 corresponding to $I_s = I_c$. Instead, the resonance of Sample A (C) stays put at $B_0 \geq 28$ μT ($B_0 \geq 9$ μT). We attribute this to flux trapping, which most likely occurs at the loop corners where the inhomogeneous bias field of the square coil is the strongest (about $1.5B_0$). Ref. 19 proposes a flux-trapping condition of the form $I_s \geq I_T \propto (J_c d)^{3/4} w^{1/2}$ where J_c is the critical current density. In the supplementary material we estimate that flux is trapped at $I_s \geq 37$ mA ($I_s \geq 11$ mA) in Sample A (C), which is below $I_c = 45$ mA ($I_c = 15$ mA).

Regarding the quality factors, we note that Sample A is overcoupled with $Q_e = 350$ much smaller than $Q_i \leq 2500$. Sample C is close to being critically coupled ($Q_e = 3500$, $Q_i \leq 3750$). Since material quality is known to affect YBCO rf loss,[20] the lower Q_e of Sample A is designed to cover a wider Q_i range more reliably. The observed Q_i variations with respect to B_0 are on the order of 10% (see supplementary material for data). Low internal dissipation is key to achieving high device sensitivity. Thus, we discuss the possible mechanisms affecting Q_i. Firstly, the resistive part of the superconductor rf surface impedance generates loss that grows with increasing T, I_s, and surface roughness.[21,22] The dielectric losses of the substrates should not play a role: both sapphire and MgO have low relative permittivity (sapphire: $\epsilon_r = 9.3$ and $\epsilon_{rz} = 11.3$ anisotropic, MgO: $\epsilon_r = 9.6$) and low dielectric loss tangents[23–25] (<4×10^{-6}) at

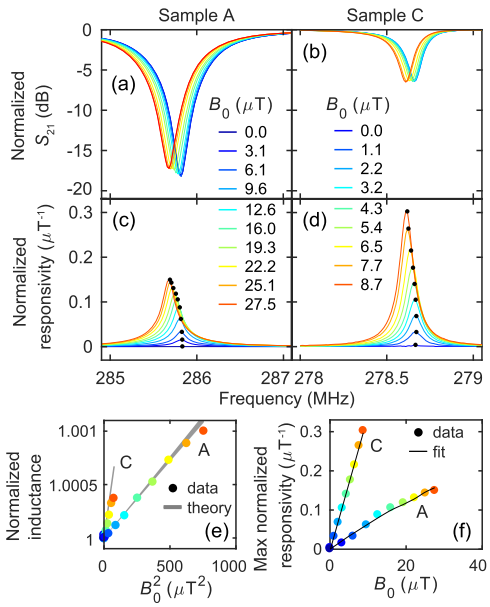

FIG. 2. High-T_c KIM characterization as functions of readout frequency and static magnetic field B_0. The measurements of Sample A [(a),(c)] and Sample C [(b),(d)] show a qualitatively similar response to a variable B_0 induced by the dc bias coil. (a),(b) The dip in the transmission S-parameter magnitude 20 $\log_{10}|2V/V_{in}|$ gives information on the changes in the L_k and dissipation in the superconducting loop. (c),(d) The responsivity $|\frac{\partial V}{\partial B_0}/V|$ is extracted from the simultaneous measurement of a 1-kHz magnetic probe tone produced by the ac bias coil. The Sample A (C) probe magnitude is 140 nT (30 nT). The responsivity maxima are indicated with dots. (e) The shift in the resonance frequency is converted into a normalized change in total inductance, and presented as a function of B_0^2. See text for the theoretical model (grey lines). (f) Maximal responsivity as a function of B_0. The solid lines are fits that are explained in the text.

$T = 77$ K. A loss mechanism related to the PCB deserves further attention: the presence of the bias coils made of resistive copper. In Ref. 9 as well as for the data presented in Figs. 2–3 for Sample A, bias coil rf decoupling is attempted with series impedances (resistance, inductance) on the order of hundreds of Ohms within the coils. This has allowed for Q_i up to 2500, but we have learned that higher values can be reached with an arrangement where the bias coils are grounded at rf and the readout is mediated by stray coupling between the KIM and the coils (see supplementary material for details). Samples B and C as well as a subsequent cooldown of Sample A (Fig. 4) have been prepared using this better method, which presumably allows for a Q_i that is limited by the intrinsic superconductor loss.

The measured device responsivities are presented in Fig. 2(c,d) as a function of the readout frequency. They are of the normalized form $|V^{-1}\partial V/\partial B_0|$: this is a convenient quantity because both V and $\partial V/\partial B_0$ experience the same gain of the readout electronics. We average these two quantities for 300 ms at each readout frequency. The measured readout frequency dependencies of $|\partial V/\partial B_0|$ are Lorentzians that peak on resonance. We use these data for the estimation of the sensor dynamic range,[9] which is approximately 11 μT (2.8 μT) for Sample A (C) at high responsivity. As expected, the responsivity vanishes at the first-order flux-insensitive points

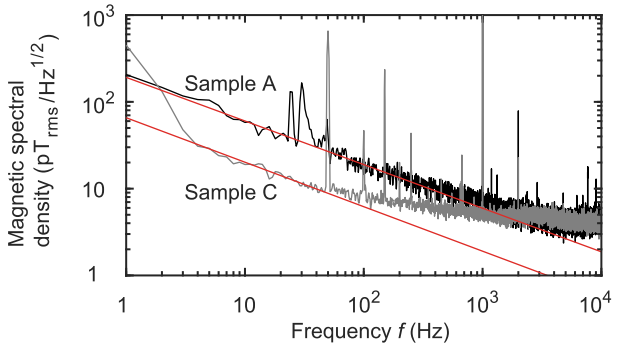

FIG. 3. Measured magnetic field noise of Samples A and C at a high readout power of − 19 dBm, − 46 dBm, respectively. The fits to the low-frequency noise (lines) are of the form $\propto f^{-0.50}$ with − 0.50 the best-fit exponent. The measurement of Sample C appears to be more susceptible to drifts that are a likely explanation for the noise rise at $f < 4$ Hz. The spectral peak at 1 kHz is a deterministic magnetic probe tone, which is used for optimal rotation of the signal quadratures. Other peaks are either due to the pick-up of rf interference, or generated by the readout electronics.

where $I_s = 0$. The peaks of $|V^{-1}\partial V/\partial B_0|$, shown as a collection in Fig. 2(f), are almost linearly proportional to B_0. If we normalize Eq. (3) in the limit of $1/\alpha_k \gg 3(I_s/I^*)^2$,

$$\left|\frac{1}{V}\frac{\partial V}{\partial B_0}\right| \approx \frac{Q_i^2 A}{2(Q_i+Q_e)}\frac{\alpha_k I_s}{L_{tot} I^{*2}}, \tag{4}$$

we obtain a responsivity model where we further assume an approximately linear mapping from B_0 into I_s [consider Eq. (2) at $m = 0$]. The theory implies that the quadratic term in the normalized inductance, $L_{tot}(B_0)/L_{tot}(0) \propto kB_0^2$ with k the slope [see Eq. (1)], is closely related to the normalized responsivity in Eq. (4): $|V^{-1}\partial V/\partial B_0| = 2Q_i^2 kB_0/(Q_i + Q_e)$. To demonstrate this relationship, we extract k from best fits to the normalized responsivity data. The fit of Sample A [Fig. 2(f)] is slightly curved because it takes into account the independently measured Q_i variation (by contrast, Sample C has a Q_i which is close to a constant). We put the k into use in theory overlays on top of the measured inductance in Fig. 2(e), and observe good agreement. The uncertainties in the overlays are calculated from the error estimates of k. The best-fit k is about six times steeper in Sample C in comparison to Sample A, which is primarily an indication

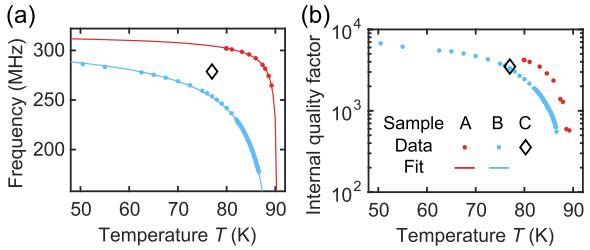

FIG. 4. Measured temperature dependencies of Samples A-C in which the film thicknesses are $d = 225$ nm, 50 nm, 75 nm, respectively. The resonance frequency (a) and the internal quality factor (b) are presented as a function of T. See text for the model used for the fits (lines).

of a higher α_k and a lower I^* resulting from the thinner film. Despite the difference in the resonance lineshape, the term in Eq. (4) related to the quality factors, $Q_i^2/(Q_i + Q_e)$, is of similar magnitude in the two KIMs [about 2000 (1900) in Sample A (C)].

To determine the magnetic field sensitivity of Samples A and C, we record time traces of V and average the squared modulus of their Fourier transform 14 − 30 times to reduce the uncertainty of the noise estimate. This type of averaging retains the noise power that is present in S_V, the spectrum of V. The trace duration is 1.0 s and the sample rate is one megasample per second (see the supplementary material for the setup and the interference peaks in S_V). Importantly, an rf carrier cancellation circuit [Fig. 1(c)] is activated now to prevent the saturation of the readout electronics. To avoid adding phase noise to V, we take the cancellation tone, the readout tone, and the reference for demodulation from the same rf generator. We measure the sensitivity at f_r as a function of P_{rf}, and we also compare B_0 bias points with a high and a vanishingly small $|\partial V/\partial B_0|$. At low P_{rf} we observe a white S_V determined by thermal noise and noise added by the preamplifiers. As we increase the power, an $S_V \propto 1/f$-like spectrum emerges and eventually dominates the voltage noise, increasing linearly with P_{rf} (see supplementary material for details). The voltage spectra at the high responsivity and at the highest P_{rf} have been converted into the magnetic domain in Fig. 3, yielding a sensitivity $|\partial V/\partial B_0|^{-1} S_V^{1/2}$ of about 4 pT/$\sqrt{\text{Hz}}$ at 10 kHz for both KIMs. The $1/f$ corner frequency is about 2 kHz (500 Hz) for Sample A (C). However, the noise of Sample C appears to scale according to a different exponent in the power law of the frequency dependence at 0.1 − 1 kHz. We can rule out direct magnetic field noise because S_V is similar at the operating point with vanishing responsivity (see supplementary material for data). The origin of the low-frequency noise mechanism is currently not fully understood.

Finally, we probe the resonances of Samples A and B at a variable temperature. The extracted $f_r(T)$ and $Q_i(T)$ are the most sensitive to T when the devices are just below T_c (Fig. 4). An analytical model[7,26]

$$\frac{f_r(T) - f_r(T_{min})}{f_r(T_{min})} \propto \lambda(T = T_{min}) - \lambda_0\left[1 - \left(\frac{T}{T_c}\right)^2\right]^{-1/2} \tag{5}$$

exists where T_{min} is the lowest T in the dataset, and $\lambda_0 = \lambda(T = 0)$. For both samples, the best fits of this form have $T_c = 90.5 \pm 0.2$ K and $\lambda(T = 77\text{ K}) \approx 1.9\lambda_0$ [Fig. 4(a)]. According to the fit, the sensitivity of f_r to T in Sample A is about − 0.64 MHz/K at $T = 77$ K. We use this information to estimate[13] that a 1 mK change in T would produce the same swing in V as a 57 nT change in B_0, at the operating point where the noise of Sample A has been measured. Furthermore, we combine the $f_r(T)$ data with geometric considerations to estimate that Samples A, B and C have $\alpha_k \simeq 0.06, 0.4, 0.16$, respectively, at $T = 77$ K. In Fig. 4(b) we deduce that the $Q_i(T)$ drop below 10^3 near T_c is a result of a remarkable increase of intrinsic rf losses.

In conclusion, we have demonstrated high-T_c kinetic inductance magnetometers with a sensitivity of 4 pT/$\sqrt{\text{Hz}}$ at 10 kHz and $T = 77$ K. They tolerate background fields of 9 − 28 μT, which is close to the Earth's field. We anticipate that changing the sensor geometry by implementing narrow constrictions[10] to reduce I_c should allow for periodical resets, enabling operation at even higher fields. This could open the road to applications in, e.g., geomagnetic exploration[27] or quantum computation[10] with electron spins or trapped

ions. The constrictions should also help to increase α_k, a likely route towards a higher responsivity. Considering the sensitivity, we would find useful a further study of the cause of the low-frequency noise, and methods to minimize it.

See supplementary material for detailed information on the samples, the experimental setup, the estimates of I_s and I_c, as well as extended measurement data.

We thank Maxim Chukharkin for fabricating Sample A, Paula Holmlund for help in sample preparation, and Juho Luomahaara and Heikki Seppä for valuable discussions. V.V., H.S., M.K. and J.H. acknowledge financial support from Academy of Finland under its Centre of Excellence Program (project no. 312059), and grants no. 305007 and 310087. S.R., A.K., D.W. and J.F.S. acknowledge financial support from the Knut and Alice Wallenberg Foundation (KAW2014.0102), the Swedish Research Council (621-2012-3673) and the Swedish Childhood Cancer Foundation (MT2014-0007). We acknowledge support from the Swedish national research infrastructure for micro and nano fabrication (Myfab) for device fabrication.

REFERENCES

[1] A. Timofeev, J. Luomahaara, L. Grönberg, A. Mäyrä, H. Sipola, M. Aikio, M. Metso, V. Vesterinen, K. Tappura, J. Ala-Laurinaho, A. Luukanen, and J. Hassel, IEEE Trans. THz Sci. Technol. **7**, 218 (2017).
[2] M. A. Lindeman, J. A. Bonetti, B. Bumble, P. K. Day, B. H. Eom, W. A. Holmes, and A. W. Kleinsasser, J. Appl. Phys. **115**, 234509 (2014).
[3] B. Ho Eom, P. K. Day, H. G. LeDuc, and J. Zmuidzinas, Nat. Phys. **8**, 623 (2012).
[4] L. Ranzani, M. Bal, K. C. Fong, G. Ribeill, X. Wu, J. Long, H.-S. Ku, R. P. Erickson, D. Pappas, and T. A. Ohki, Appl. Phys. Lett. **113**, 242602 (2018).
[5] G. Wang, C. L. Chang, S. Padin, F. Carter, T. Cecil, V. G. Yefremenko, and V. Novosad, J. Low. Temp. Phys. **193**, 134 (2018).
[6] J. v. Rantwijk, M. Grim, D. v. Loon, S. Yates, A. Baryshev, and J. Baselmans, IEEE Trans. Microw. Theory Techn. **64**, 1876 (2016).
[7] K. Sato, S. Ariyoshi, S. Negishi, S. Hashimoto, H. Mikami, K. Nakajima, and S. Tanaka, J. Phys.: Conf. Ser. **1054**, 012053 (2018).
[8] H. Sipola, J. Luomahaara, A. Timofeev, L. Grönberg, A. Rautiainen, A. Luukanen, and J. Hassel, arXiv:1810.03848 [physics] (2018).
[9] J. Luomahaara, V. Vesterinen, L. Grönberg, and J. Hassel, Nat. Commun. **5**, 4872 (2014).
[10] A. T. Asfaw, E. I. Kleinbaum, T. M. Hazard, A. Gyenis, A. A. Houck, and S. A. Lyon, Appl. Phys. Lett. **113**, 172601 (2018).
[11] A. Ghirri, C. Bonizzoni, D. Gerace, S. Sanna, A. Cassinese, and M. Affronte, Appl. Phys. Lett. **106**, 184101 (2015).
[12] M. I. Faley, J. Dammers, Y. V. Maslennikov, J. F. Schneiderman, D. Winkler, V. P. Koshelets, N. J. Shah, and R. E. Dunin-Borkowski, Supercond. Sci. Technol. **30**, 083001 (2017).
[13] J. Zmuidzinas, Annu. Rev. Condens. Matter Phys. **3**, 169 (2012).
[14] M. R. Vissers, J. Hubmayr, M. Sandberg, S. Chaudhuri, C. Bockstiegel, and J. Gao, Appl. Phys. Lett. **107**, 062601 (2015).
[15] M. R. Vissers, J. Gao, D. S. Wisbey, D. A. Hite, C. C. Tsuei, A. D. Corcoles, M. Steffen, and D. P. Pappas, Appl. Phys. Lett. **97**, 232509 (2010).
[16] G. Ghigo, D. Botta, A. Chiodoni, R. Gerbaldo, L. Gozzelino, F. Laviano, B. Minetti, E. Mezzetti, and D. Andreone, Supercond. Sci. Technol. **17**, 977 (2004).
[17] W. Hattori, T. Yoshitake, and S. Tahara, IEEE Trans. Appl. Supercond. **8**, 97 (1998).
[18] A. Megrant, C. Neill, R. Barends, B. Chiaro, Y. Chen, L. Feigl, J. Kelly, E. Lucero, M. Mariantoni, P. J. J. O'Malley, D. Sank, A. Vainsencher, J. Wenner, T. C. White, Y. Yin, J. Zhao, C. J. Palmstrøm, J. M. Martinis, and A. N. Cleland, Appl. Phys. Lett. **100**, 113510 (2012).
[19] J. Z. Sun, W. J. Gallagher, and R. H. Koch, Phys. Rev. B **50**, 13664 (1994).
[20] J. H. Lee, Y. B. Ko, and S. Y. Lee, Supercond. Sci. Technol. **16**, 386 (2003).
[21] A. G. Zaitsev, R. Schneider, G. Linker, F. Ratzel, R. Smithey, P. Schweiss, J. Geerk, R. Schwab, and R. Heidinger, Rev. Sci. Instrum. **73**, 335 (2002).
[22] L. M. Wang, C.-C. Liu, M.-Y. Horng, J.-H. Tsao, and H. H. Sung, J. Low. Temp. Phys. **131**, 551 (2003).
[23] J. Krupka, R. Geyer, M. Kuhn, and J. Hinken, IEEE Trans. Microw. Theory Techn. **42**, 1886 (1994).
[24] S. N. Buckley, P. Agnew, and G. P. Pells, J. Phys. D: Appl. Phys. **27**, 2203 (1994).
[25] R. C. Taber and C. A. Flory, IEEE Trans. Ultrason., Ferroelectr., Freq. Control **42**, 111 (1995).
[26] J. H. Lee, W. I. Yang, M. J. Kim, J. C. Booth, K. Leong, S. Schima, D. Rudman, and S. Y. Lee, IEEE Trans. Appl. Supercond. **15**, 3700 (2005).
[27] B. Schmidt, J. Falter, A. Schirmeisen, and M. Mück, Supercond. Sci. Technol. **31**, 075006 (2018).